Stability Analysis of DC Distribution System Considering Stochastic State of Electric Vehicle Charging Stations

Qiang Fu, *Member, IEEE*, Wenjuan Du, *Member, IEEE*, Haifeng Wang, *Senior Member, IEEE*, and Xianyong Xiao, *Senior Member, IEEE*

***Abstract*—A DC distribution system integrated with electric vehicle charging stations (EVCSs) is typically constructed to satisfy the large power exchange demand of electric vehicles (EVs). However, the stochastic operating state of the EVCSs results in difficulties in the stability analysis of the DC distribution system. In this study, a linearized model of the DC distribution system connected with multiple EVCSs is established, which considers the charging and the discharging states of the EVCSs. Based on the similarity transformation, this study theoretically verifies the generalized conclusion that a DC distribution system has a higher possibility of instability if the EVCSs are in the charging rather than the discharging state, and that the system stability is the worst if all the EVCSs operate at the maximum charging state. Moreover, a method to quickly evaluate the stability region of the DC distribution system is proposed. It can provide a numerical instability risk estimation of a complex DC distribution system considering all the possible states of the EVCSs. Lastly, the conclusions are validated by two SIMULINK cases, and the application of the numerical instability risk estimation to the DC distribution system is demonstrated.**

***Index Terms*—DC distribution system, electric vehicle charging stations, instability risk estimation, stability analysis.**

NOMENCLATURE

C_{fk}	Capacitance of output filter of k^{th} DC/DC converter
C_{Lk}	Voltage-regulator capacitance of k^{th} battery
$C_{Vk}(s) = K_{Vpk} + K_{Vik}s^{-1}$	Transfer function of the outer voltage PI controller for the k^{th} DC/DC converter
$C_{Ik}(s) = K_{Ipk} + K_{Iik}s^{-1}$	Transfer function of the inner current PI controller for the k^{th} DC/DC converter
d_{Lk}	Duty ratio of the k^{th} DC/DC converter
i_{dck}	DC current injected into C_{fk}
i_{fk}	DC current output from C_{fk}
i_{pcc}	DC current injected into the AC/DC converter
i_{Lk}	Load current of k^{th} battery
L_{fk}	Inductance of output filter of k^{th} DC/DC converter
L_{Lk}	Inductance of line connecting the k^{th} DC/DC converter and battery
P_{pcc}	Total active power output from the AC/DC converter
P_{Lk}	Load active power of k^{th} battery
R_{fk}	Resistance of output filter of the k^{th} DC/DC converter
R_{Lk}	Resistance of the line connecting the k^{th} DC/DC converter and battery
V_{dck}	DC voltage of the k^{th} EVCS
V_{fk}	DC voltage across C_{fk}
V_{pcc}	DC voltage of the AC/DC converter
V_{Lk}	DC voltage across C_{Lk}
X	Reactance of AC filter of the AC/DC converter
$\mathbf{A}_k$, $\mathbf{B}_k$, and $\mathbf{C}_k$	State-space matrix, control, and output vectors of the k^{th} EVCS utilizing the full-order model
$\mathbf{A}_E$, $\mathbf{B}_E$, and $\mathbf{C}_E$	State-space matrix, control, and output vectors of *M* EVCSs utilizing the reduced-order model
$\mathbf{A}_D$	State-space matrix of the DC distribution system
$\mathbf{Z}$	Impedance matrix of the DC network
ρ_k	Eigenvalues of $\mathbf{Z}$
$diag()$	Diagonal block matrix
Superscript *ref*	Control references of state variables
Subscript 0	Value of a variable at the steady state
Δ	Small increment of a variable or variable vector
$\otimes$	Kronecker product
Re	Real part of a variable

Manuscript received December 18, 2020; revised May 25, 2021 and August 31, 2021; accepted October 3, 2021. Date of publication October 19, 2021; date of current version April 19, 2022. This work was supported by the Engineering Special Team of Sichuan University on New Energy Power Systems and financially supported by the Natural Science Foundation of China under Grant 52077144. Paper no. TPWRS-02074-2020. *(Corresponding author: Wenjuan Du.)*

Qiang Fu is with the School of EEEng, Sichuan University - Wangjiang Campus, Chengdu, Sichuan 610065, China (e-mail: fuqiang346@qq.com).

Wenjuan Du and Haifeng Wang are with the Sichuan University - Wangjiang Campus, Chengdu, Sichuan 610065, China (e-mail: ddwenjuan@qq.com; hfwang60@qq.com).

Xianyong Xiao is with the College of Electrical Engineering and Information Technology, Sichuan University, Chengdu, Sichuan 610065, China (e-mail: xiaoxianyong@163.com).

Color versions of one or more figures in this article are available at https://doi.org/10.1109/TPWRS.2021.3121316.

Digital Object Identifier 10.1109/TPWRS.2021.3121316

I. Introduction

In RECENT years, environmental pollution has gained considerable attention globally. Consequently, electric vehicles (EVs) have been rapidly developed as an effective solution. As the number of EVs connected to the DC distribution system increases, a greater number of studies on the EV charging stations (EVCSs) and DC network have been conducted with the aim of obtaining a more convenient and stable power supply [1]–[3].

Hitherto, investigations on the impact of EVCS integration on the DC distribution system have been focused on two main areas. The first is the impact of the steady-state operating conditions of the DC distribution system, such as the optimization of economy, control, and reliability. In this regard, EVCSs are generally considered to be constant power loads, and studies have been majorly aimed at reducing the costs during planning by considering the economic and traffic conditions [4]–[9]. The second area is the impact of the dynamics of EVCSs and the DC network. It has been shown that the control loop of the EVCSs determines their self-stability, which rarely interacts with the DC network itself. The filter loop of the EVCSs is the primary factor interacting with the DC network and which results in instability of the DC distribution system [10]–[11]. Assuming a perfectly performing converter control system, an individual EVCS can be considered to be a constant power load (CPL), enabling the modeling of the individual EVCS dynamics as a negative resistance within the DC distribution system. Based on the impedance model-based analysis, this model suggests that EVCS integration degrades network stability [12]–[14]. By developing advanced control strategies to alter the EVCS dynamics, the stability of the DC distribution system can be considerably improved [15]–[16]. Regarding the topology and the parameters of the DC network, an examination of the stability of a cascaded network with multiple CPLs [17] concluded that improving the planned topology of the DC network considerably enhanced the network stability. In [18], the impact of the transmission line and the EVCS output power on the stability of a DC distribution system was investigated using eigenvalue migration plots. It was found that when the cable length and/or the output power increased, the network stability decreased. In another study [19], it was found that the stability of a DC distribution system was affected by the number of parallelly connected converters. It has been demonstrated that the dynamics of both the EVCSs and the DC network affect the stability of the DC distribution system, indicating that the EVCSs and the DC networks should be carefully designed to eliminate such instability.

For practical application, an index of instability risk is very useful. When the EVCSs are modeled as constant power sources in the stability analysis, the index of instability risk derived from stability analysis cannot be used to identify the instability danger caused by the dynamics of the EVCSs and DC network [12]–[14]. In [20], an index of instability risk was proposed when the dynamics of output filter were considered, though the EVs were represented by constant power sources. The proposed index can be used to assess the instability danger caused by the output filter. However, two important factors that may affect the stability of the DC distribution system were not considered in [20]. The first one is the entire dynamics of the EVCSs. The second affecting factor is the general topology of the DC network.

In [10] and [21], the authors analytically examined the stability of a DC distribution system as affected by the EVCSs. In the examination, entire dynamics of the EVCSs were considered. However, with the entire dynamics of the EVCSs being considered, the mathematical model of the DC distribution system is complex and high-dimensional, which makes the theoretical analysis of system stability very difficult. Hence, stability analysis in [10] and [21] was carried out based on the assumption that the dynamics of the EVCSs were identical. The assumption enabled the simplification of the mathematical model of the DC distribution system for the stability analysis. In [10], the DC distribution system with a general network topology was considered. In [21], two typical network topologies were compared. However, the assumption of identical dynamics of the EVCSs is too strong to be true in practice, though the assumption is applicable in the case of planning the DC distribution system. Another gap of study left by the work in [10] and [21] is the impact of variable operating state of the EVCSs.

The focus of this study is the stochastic operating state of the EVCSs and its impact on the stability of the DC distribution system which are dominated by dynamics of the EVCSs. Conventionally, an EVCS is often to provide the service for a particular type of the EVs. In the DC distribution system, an EVCS should provide the service for any types of the EVs, where the charging power is variable, depending on the type of the EV being connected. Thus, the charging power of the EVCS varies when it is connected to different type of the EVs. Under this condition, the charging power of each EVCS is stochastic since there is no constraints on the type of the EVs that can receive the service. Hence, the stochastic operating state of the EVCSs mainly implies the randomly variable charging power of the EVCSs. The other parameters of the EVCSs, such as those of control loops and transmission lines are not stochastic. They are constant and can be determined by a realistic DC distribution system. Thus, the traditional modeling method is also effective for establishing the linearized model of an EVCS in this study. Differently, the charging power of the established model of the EVCS is stochastic, which results in differences in state-space matrixes among the EVCSs.

In this paper, the entire dynamics and random variation of operating state of the EVCSs are considered in examining the stability of a DC distribution. Based on the examination, an index is proposed for the quick evaluation of the instability risk caused by the EVCSs. Main contributions of the paper are as follows.

Firstly, in the stability analysis, the assumption of identical dynamics of the EVCSs made in [10] and [21] is removed. The limitation of the DC network topology in [20] is eliminated, and the stability of a DC distribution system with any network topology can be considered. In addition, in the stability analysis, entire dynamics of the EVCSs are included. To reduce the complexity of the full-order model of DC distribution system, dynamic equivalent model, rather that the simplified dynamics model, is derived and used for the stability analysis. Hence,

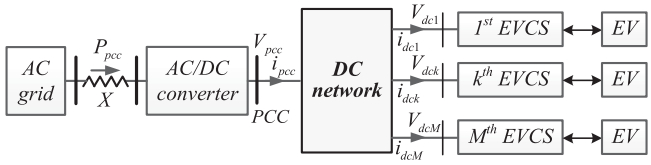

Fig. 1. Configuration of a DC distribution system connected with *M* EVCSs.

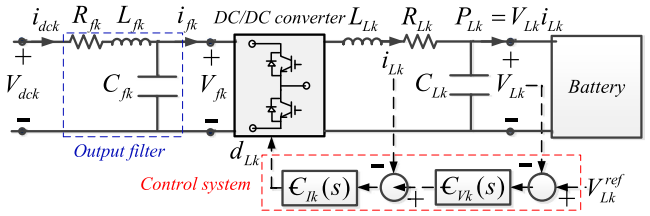

Fig. 2. Configuration of the k^{th} standalone EVCS.

the conclusions obtained from the stability analysis are more generally applicable.

Secondly, for the practical application, the instability risk index derived by ignoring the dynamics of the EVCSs is inapplicable to detect the instability caused by the dynamics of the EVCSs. The instability risk index derived for particular network topology [20] or on the basis of assumed unified property of the EVCSs [10], [21] limits the scalability of the DC distribution system. The index of instability risk proposed in the paper is based on the estimation of the oscillation modes of the DC distribution system with general network topology, entire dynamics and randomly variable operating state (charging power) of the EVSCs. The applicability of the proposed index is of better scalability.

The remainder of this paper is organized as follows. Section II introduces the configuration and establishes the linearized model of a DC distribution system connected with the EVCSs. In Section III, the impact of the different states of the EVCSs on the stability of the DC distribution system is clarified, and the method to quickly evaluate the stability risk of the DC distribution system is proposed. In Section IV, two examples based on the MATLAB SIMULINK (Math Works, USA) are presented to validate and demonstrate the analytical conclusions and potential applications. In the final section, the major conclusions and contributions of the study are summarized.

II. Linearized Model of the DC Distribution System Connected With EVCSs

Fig. 1 shows a DC distribution system used to satisfy the large charging demand of EVs. *M* EVCSs are connected to the point of common coupling (PCC) through the DC network. Fig. 2 shows a commonly used model of a standalone EVCS [18], [21]. Herein, electronic topologies of the AC/DC and DC/DC converters can be separately found in documentation provided by the MATLAB [22]–[23].

A. Linearized Model of M EVCSs

For the circuit in Fig. 2, the following voltage and current equations can be obtained:

$$V_{dck}=R_{fk}i_{dck}+L_{fk}\frac{di_{dck}}{dt}+V_{fk},\ i_{dck}=i_{fk}+C_{fk}\frac{dV_{fk}}{dt}$$
$$d_{Lk}V_{fk}=R_{Lk}i_{Lk}+L_{Lk}\frac{di_{Lk}}{dt}+V_{Lk}$$
$$i_{fk}=d_{Lk}i_{Lk}=d_{Lk}C_{Lk}\frac{dV_{Lk}}{dt}+d_{Lk}\frac{P_{Lk}}{V_{Lk}} \quad (1)$$

The control system of the DC/DC converter can be expressed by the following equations:

$$\frac{dx_{Vk}}{dt}=K_{Vik}\left(V_{Lk}^{ref}-V_{Lk}\right)$$
$$\frac{dx_{Ik}}{dt}=K_{Iik}x_{Vk}+K_{Iik}K_{Vpk}\left(V_{Lk}^{ref}-V_{Lk}\right)-K_{Iik}i_{Lk}$$
$$d_{Lk}=x_{Ik}+K_{Ipk}x_{Vk}+K_{Ipk}K_{Vpk}\left(V_{Lk}^{ref}-V_{Lk}\right)-K_{Ipk}i_{Lk} \quad (2)$$

By linearizing (1) and (2), the following full-order state-space model of the k^{th} EVCS is obtained (Details can be found in Appendix A.) [20]–[21]:

$$\frac{d}{dt}\mathbf{\Delta X}_k=\mathbf{A}_k\mathbf{\Delta X}_k+\mathbf{B}_k\Delta V_{dck}$$
$$\Delta i_{dck}=\mathbf{C}_k\mathbf{\Delta X}_k \quad (3)$$

It can be seen from (1) and (2) that the dynamics of the EVCS are determined by the filter and the control subsystems. At the steady state, the transmitted power of the EVCS is directly determined by the charging demand of the EVs, which is positive when the EVs absorb power and is negative when they output power. Based on (3), the linearized model of *M* EVCSs is obtained as:

$$s\mathbf{X}_E=\mathbf{A}_E\mathbf{X}_E+\mathbf{B}_E\mathbf{\Delta V_{dc}},\mathbf{\Delta I_{dc}}=\mathbf{C}_E\mathbf{X}_E \quad (4)$$

where $\mathbf{X}_E=[\mathbf{X}_1\ \ldots\ \mathbf{X}_M]^T$, $\mathbf{\Delta I_{dc}}=[\Delta i_{dc1}\ \ldots\ \Delta i_{dcM}]^T$, $\mathbf{\Delta V_{dc}}=[\Delta V_{dc1}\ \ldots\ \Delta V_{dcM}]^T$.

$$\mathbf{A}_E=\begin{bmatrix}\mathbf{A}_1 & & \\ & \ddots & \\ & & \mathbf{A}_M\end{bmatrix},\mathbf{B}_E=\begin{bmatrix}\mathbf{B}_1 & & \\ & \ddots & \\ & & \mathbf{B}_M\end{bmatrix},\mathbf{C}_E=\begin{bmatrix}\mathbf{C}_1 & & \\ & \ddots & \\ & & \mathbf{C}_M\end{bmatrix}.$$

B. Linearized Model of the DC Distribution System

The central AC/DC converter is connected to the AC power system and operated as a controlled DC voltage power port [24]–[25]. Considering that the capacity of the AC power system is much larger than that of the DC distribution system, the DC voltage of the central AC/DC converter can be regarded as constant, i.e., $\Delta V_{pcc}=0$. The AC/DC converter enables a

bidirectional exchange of energy between the DC distribution system and the AC power system. Therefore, regarding any topology of the DC network, as indicated in Fig. 1, the following impedance matrix represents the transfer function between $\Delta\mathbf{V}_{dc}$ and $\Delta\mathbf{I}_{dc}$ at frequency ω_0.

$$\Delta\mathbf{V}_{dc} = -\mathbf{Z}(j\omega_0)\Delta\mathbf{I}_{dc} \tag{5}$$

where the elements of the matrix $\mathbf{Z}(j\omega_0)$ are positive, and $\mathbf{Z}(j\omega_0)$ is denoted as $\mathbf{Z}$ for simplification.

Combining (4) with (5), the state-space matrix of the DC distribution system with *M* EVCSs can be expressed as

$$\mathbf{A}_D = \mathbf{A}_E - \mathbf{B}_E\mathbf{Z}\mathbf{C}_E = diag(\mathbf{A}_k) - [\mathbf{Z}\otimes\mathbf{I}]diag(\mathbf{B}_k\mathbf{C}_k) \tag{6}$$

where $\mathbf{A}_D \in R^{6M\times 6M}$, $\mathbf{B}_k\mathbf{C}_k \in R^{6\times 6}$, and $\mathbf{I}$ is a 6×6 unit matrix.

It is observed from (6) that the stability of the DC distribution system is influenced by two factors: the dynamics of *M* EVCSs, represented by $\mathbf{A}_E$, and those of the DC network, represented by $\mathbf{B}_E\mathbf{Z}\mathbf{C}_E$. The dimensions of $\mathbf{A}_D$ increase with the increasing number of the EVCSs, complicating the stability assessment of the DC distribution system. For convenience, an equivalent model is derived in the next section to determine the stability region, and an index is proposed to numerically evaluate the instability risk of the DC distribution system by considering the stochastically varying operating states of the EVCSs. This can reduce the complexity of the stability evaluation.

III. Stability Analysis of the DC Distribution System

In engineering, EVCSs are installed according to unified standards, such that the filter parameters of each EVCS are the same, yielding

$$C_{f1} = C_{fk}, L_{f1} = L_{fk}, R_{f1} = R_{fk}, k \in [1, M] \tag{7}$$

It can be seen from (3) that two factors affect $\mathbf{A}_k$. The first one is the parameters of the transmission line and the control loop of the EVCS, which are constant in a specific DC network. The second affecting factor is the charging power of the EVCS, which relies on the charging demand of the connected EV. Charging power does not belong to state variables of the state-space model of the EVCS, so that does not affect the establishment of the state-space model of (3). Considering the charging power of each EVCS is variable, $\mathbf{A}_k$ varies mainly with the changes of the charging power of the EVCS. Therefore, the number of randomly variable charging powers of the M EVCSs is M. At a given time, Denote $P_{\min}$ and $P_{\max}$ as the minimum and maximum charging power among M EVCSs. If the charging power of the connected EV is greater than the nominal power of the EVCS, the nominal power is taken as the maximum charging power. Otherwise, the maximum charging power equals to the maximum charging demand among the connected EVs. Thus, the charging power of the k^{th} EVCS can be expressed as

$$P_{Lk} = P_{\min} + \Delta P_k = P_{\max} - (P_{div} - \Delta P_k) \tag{8}$$

where $P_{div} = P_{\max} - P_{\min}$, ΔP_k is the increment of charging power from $P_{\min}$, and $P_{div} \geq \Delta P_k \geq 0$, $k = 1, 2, \ldots, M$.

Denote $\mathbf{A}_{\min}$and $\mathbf{A}_{\max}$ as the state-space matrices of the EVCS when it operates with the minimum and maximum charging power $P_{\min}$ and $P_{\max}$, respectively. $\mathbf{A}_{\min}$ and $\mathbf{A}_{\max}$ can be obtained by substituting the values of various variables of the EVCS at minimum and maximum charging states in (3), respectively. Thus, for the k^{th} EVCS, the deviation between $\mathbf{A}_k$ and $\mathbf{A}_{\min}$, is mainly caused by ΔP_k, which can be denoted as $\mathbf{A}_{pk}$. With those definitions introduced above, the state-space model of the EVCS can be expressed as

$$\mathbf{A}_k = \mathbf{A}_{\min} + \mathbf{A}_{pk} = \mathbf{A}_{\max} - (\mathbf{A}_{div} - \mathbf{A}_{pk}) \tag{9}$$

where $\mathbf{A}_{pk}$ and $\mathbf{A}_{div}$ are the increment matrices, which are caused by ΔP_k and P_{div}, respectively.

Based on (9), the state-space matrix of the DC distribution system with *M* EVCSs can be expressed from (6) as

$$\begin{aligned}\mathbf{A}_D &= diag(\mathbf{A}_{\min}) + diag(\mathbf{A}_{pk}) - [\mathbf{Z}\otimes\mathbf{I}]diag\left(\mathbf{B}_k\mathbf{C}_k\right)\\ &= diag\left(\mathbf{A}_{\max}\right) - diag\left(\mathbf{A}_{div} - \mathbf{A}_{pk}\right)\\ &\quad - [\mathbf{Z}\otimes\mathbf{I}]\,diag\left(\mathbf{B}_k\mathbf{C}_k\right)\end{aligned} \tag{10}$$

A. Equivalent Model of the DC Distribution System

There exists a matrix $\mathbf{P}_c$ [26] such that

$$\mathbf{P}_c\mathbf{Z}{\mathbf{P}_c}^{-1} = diag(\rho_k) \tag{11}$$

where $\mathbf{P}_c{\mathbf{P}_c}^{-1} = \mathbf{I}$, and

$$\mathbf{P}_c = \begin{bmatrix} p_{11} & p_{12} & \cdots & p_{1M}\\ p_{21} & p_{22} & \cdots & p_{2M}\\ \vdots & & & \\ p_{M1} & p_{M2} & \cdots & p_{MM}\end{bmatrix}, {\mathbf{P}_c}^{-1} = \begin{bmatrix} v_{11} & v_{12} & \cdots & v_{1M}\\ v_{21} & v_{22} & \cdots & v_{2M}\\ \vdots & & & \\ v_{M1} & v_{M2} & \cdots & v_{MM}\end{bmatrix}$$

We define the following similarity transformation matrix:

$$\mathbf{P} = \mathbf{P}_c\otimes\mathbf{I}, \mathbf{P}^{-1} = {\mathbf{P}_c}^{-1}\otimes\mathbf{I} \tag{12}$$

From (12), this yields

$$\mathbf{P}\mathbf{P}^{-1} = diag(\mathbf{I}) \tag{13}$$

In addition, making a similar transfer of the first and second equation of (10) yields

$$\begin{aligned}\mathbf{P}\mathbf{A}_D\mathbf{P}^{-1} &= \mathbf{P}diag\left(\mathbf{A}_{\min}\right)\mathbf{P}^{-1} + \mathbf{P}diag\left(\mathbf{A}_{pk}\right)\mathbf{P}^{-1}\\ &\quad - \mathbf{P}\left[\mathbf{Z}\otimes\mathbf{I}\right]diag\left(\mathbf{B}_k\mathbf{C}_k\right)\mathbf{P}^{-1}\\ &= diag\left(\mathbf{A}_{\min}\right) - diag\left(\rho_k\mathbf{I}\right)diag\left(\mathbf{B}_k\mathbf{C}_k\right)\\ &\quad + \mathbf{P}\mathbf{A}_{sto1}\mathbf{P}^{-1}\\ \mathbf{P}\mathbf{A}_D\mathbf{P}^{-1} &= \mathbf{P}diag\left(\mathbf{A}_{\max}\right)\mathbf{P}^{-1} - \mathbf{P}diag\left(\mathbf{A}_{div} - \mathbf{A}_{pk}\right)\mathbf{P}^{-1}\\ &\quad - \mathbf{P}\left[\mathbf{Z}\otimes\mathbf{I}\right]diag\left(\mathbf{B}_k\mathbf{C}_k\right)\mathbf{P}^{-1}\\ &= diag\left(\mathbf{A}_{\max}\right) - diag\left(\rho_k\mathbf{I}\right)diag\left(\mathbf{B}_k\mathbf{C}_k\right)\\ &\quad - \mathbf{P}\mathbf{A}_{sto2}\mathbf{P}^{-1}\end{aligned} \tag{14}$$

where $\mathbf{A}_{sto1} = diag(\mathbf{A}_{pk})$, and $\mathbf{A}_{sto2} = diag(\mathbf{A}_{div} - \mathbf{A}_{pk})$.

Hence, the state-space matrix of the DC distribution system, $\mathbf{A}_D$, is similar to $\mathbf{P}\mathbf{A}_D\mathbf{P}^{-1} = diag(\mathbf{A}_{\min} - \rho_k\mathbf{B}_1\mathbf{C}_1) + \mathbf{P}\mathbf{A}_{sto1}\mathbf{P}^{-1}$ and $\mathbf{P}\mathbf{A}_D\mathbf{P}^{-1} = diag(\mathbf{A}_{\max} - \rho_k\mathbf{B}_1\mathbf{C}_1) - \mathbf{P}\mathbf{A}_{sto2}\mathbf{P}^{-1}$.

B. Stability Region of the DC Distribution System

Equation (14) indicates that the minimum and maximum charging powers of the EVCSs, the eigenvalues of the DC network, and the stochastic parts of the EVCSs collectively determine the stability of the DC distribution system. Thus, the theorem below can help us clarify how these factors restricts stability of the DC distribution system.

Theorem [27]: *If* λ_{aj} *and* λ_{bj}, *where* $j = 1, 2, \ldots, m$, *are eigenvalues of* $\mathbf{A}_a$ *and* $\mathbf{A}_b$, *respectively, and satisfy* $\mathrm{Re}[\lambda_{a1}] \geq \mathrm{Re}[\lambda_{a2}] \geq \ldots \geq \mathrm{Re}[\lambda_{am}]$, $\mathrm{Re}[\lambda_{b1}] \geq \mathrm{Re}[\lambda_{b2}] \geq \ldots \geq \mathrm{Re}[\lambda_{bm}]$, *then the eigenvalues of* $\mathbf{A}_a + \mathbf{A}_b$, λ_{abj} *have the following restrictions:*

$$\mathrm{Re}[\lambda_{aj}] + \mathrm{Re}[\lambda_{b1}] \geq \mathrm{Re}[\lambda_{abj}] \geq \mathrm{Re}[\lambda_{aj} + \lambda_{bm}] \tag{15}$$

Subsequently, (15) is applied in determining the stability region of the DC distribution system as follows.

First, the eigenvalues of $\mathbf{A}_{\min} - \rho_k \mathbf{B}_1 \mathbf{C}_1$ are calculated as a vector, $\lambda_{\min k} = [\lambda_{\min 1k} \ldots \lambda_{\min 6k}]$, and those of $\mathbf{A}_{\max} - \rho_k \mathbf{B}_1 \mathbf{C}_1$ are calculated as a vector, $\lambda_{\max k} = [\lambda_{\max 1k} \ldots \lambda_{\max 6k}]$. Arranging ρ_k as $\mathrm{Re}[\rho_1] \geq \mathrm{Re}[\rho_k] \geq \ldots \geq \mathrm{Re}[\rho_M]$ and considering that $\mathbf{B}_1 \mathbf{C}_1$ is a positive definite matrix yields

$$\begin{aligned} &\mathrm{Re}\left[\lambda_{\min 1}\right] \leq \mathrm{Re}\left[\lambda_{\min 2}\right] \leq \ldots \leq \mathrm{Re}[\lambda_{\min M}] \\ &\mathrm{Re}[\lambda_{\max 1}] \leq \mathrm{Re}[\lambda_{\max 2}] \leq \ldots \leq \mathrm{Re}[\lambda_{\max M}] \end{aligned} \tag{16}$$

Considering that the minimum and maximum values of $\mathbf{A}_{pk}$ are $\mathbf{0}$ and $\mathbf{A}_{div}$, the minimum and maximum eigenvalue vectors of $\mathbf{P}\mathbf{A}_{pk}\mathbf{P}^{-1}$ and $\mathbf{P}(\mathbf{A}_{div} - \mathbf{A}_{pk})\mathbf{P}^{-1}$ are $\mathbf{0}$ and λ_{div}, where, λ_{div} is the eigenvalue vector of $\mathbf{A}_{div}$.

The eigenvalues of $\mathbf{P}\mathbf{A}_{pk}\mathbf{P}^{-1}$ are then calculated as a vector, $\lambda_{pk} = [\lambda_{p1k} \ldots \lambda_{p6k}]$, and those of $\mathbf{P}(\mathbf{A}_{div} - \mathbf{A}_{pk})\mathbf{P}^{-1}$ are calculated as a vector, $\lambda_{dpk} = [\lambda_{dp1k} \ldots \lambda_{dp6k}]$.

The realistic modes of the DC distribution system, i.e., the eigenvalues of $\mathbf{A}_D$, are denoted as M vectors $\lambda_{d1}, \lambda_{dk}, \ldots, \lambda_{dM}$, where $\lambda_{dk} = [\lambda_{d1k} \ldots \lambda_{d6k}]$. The following restrictions can be obtained from (15) and (16) as

$$\begin{aligned} &\mathrm{Re}[\lambda_{\min k}] \leq \mathrm{Re}[\lambda_{dk}] \leq \mathrm{Re}[\lambda_{\min k} + \lambda_{div}] \\ &\mathrm{Re}\left[\lambda_{\max k} - \lambda_{div}\right] \leq \mathrm{Re}[\lambda_{dk}] \leq \mathrm{Re}[\lambda_{\max k}] \end{aligned} \tag{17}$$

Equation (17) can be accurately rewritten as

$$\begin{aligned} &\max\left[\mathrm{Re}[\lambda_{\min k}], \mathrm{Re}[\lambda_{\max k} - \lambda_{div}]\right] \leq \mathrm{Re}[\lambda_{dk}] \\ &\leq \min\left[\mathrm{Re}\left[\lambda_{\min k} + \lambda_{div}\right], \mathrm{Re}[\lambda_{\max k}]\right] \end{aligned} \tag{18}$$

It is time-consuming to calculate λ_{div} and make comparisons in (18) due to the stochastic operating state of the EVCSs. Therefore, we can simplify the restrictions in (18) as

$$\mathrm{Re}[\lambda_{\min k}] \leq \mathrm{Re}[\lambda_{dk}] \leq \mathrm{Re}[\lambda_{\max k}] \tag{19}$$

The restrictions given in (19) hold on for the DC distribution system with any topology. It can be seen from (10) that the state-space matrix of the DC distribution system is affected by the state-space models of the EVCSs, $\mathbf{A}_k$, $\mathbf{B}_k$, $\mathbf{C}_k$, and the impedance matrix of the DC network, $\mathbf{Z}$. In the derivation from (11) to (21), no assumption is made about $\mathbf{Z}$. Therefore, the conclusion of (19) is applicable to the DC distribution system with any topology. For clarification, Fig. 3 illustrates the stability region of the DC distribution system (Details of Fig. 3 are presented in Appendix B).

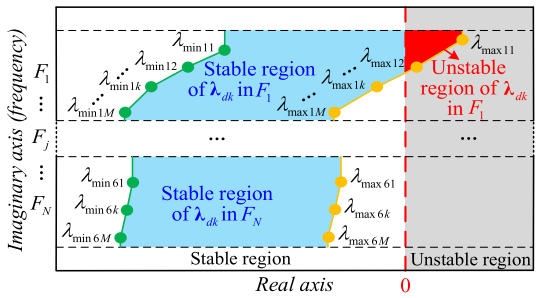

Fig. 3. Illustration about the stability region of the DC distribution system.

It can be seen from Fig. 3 that the left and right boundaries of the stability region are dependent on the locations of $\lambda_{\min k}$ and $\lambda_{\max k}$, which are indicated by the green and orange circles, respectively. The left boundary is formed by connecting $\lambda_{\min k}$ with green lines, and the right boundary is formed by connecting $\lambda_{\max k}$ with the orange lines. The stability region indicates the possible locations of λ_{dk} when the EVCSs are in the stochastic state. Regarding a selected frequency range, F_j, the stability region in F_j includes a stable region and an unstable region. They are indicated by the blue and red areas, respectively. The boundary between the stable and unstable regions is indicated by red dotted line in Fig. 3, on which the damping of oscillation modes is zero. If the oscillation modes are on the left-hand side of the dotted line, the damping of oscillation mode is positive. If an oscillation mode is on the right-hand side of the dotted line, its damping is negative and the DC distribution system is unstable.

The DC distribution system is in the danger of instability when the right boundary of the stability region exceeds the red dotted line in Fig. 3. It indicates that at least one operating state can cause instability of the DC distribution system. The larger the area of the unstable region is, the higher the risk of instability is. In order to numerically evaluate the instability risk of the DC distribution system in the selected frequency range F_j, following instability risk index RI_j is proposed:

$$RI_j = \frac{\text{Unstable region in } F_j}{\text{Stable and Unstable regions in } F_j} \tag{20}$$

In (20), we consider that the charging power of the EVs is stochastic. Thus, the charging power of each of the EVCSs is stochastically distributed in the range $[P_{\min}, P_{\max}]$. In addition, probability distribution within $[P_{\min}, P_{\max}]$ is the same. Thus, if $RI_j = 0\%$, the right boundary in Fig. 3 is on the left-hand side of the red dotted line, indicating that there is no instability risk in the frequency range. If $RI_j = 100\%$, the left boundary exceeds the red dotted line, indicating that the system must be unstable.

If probability distribution of the charging power of the EVCSs in the range $[P_{\min}, P_{\max}]$ is different, the probability of the locations of λ_{dk} in the stability region is variable. In this case, the stability region in the frequency range F_j can be divided

into stable and unstable sub-regions. Denote K_U and K_T as the number of the unstable sub-regions, and the total number of unstable and stable sub-regions respectively. If the possibility of locations of λ_{dk} in the i^{th} sub-region is μ_i, $i = 1, 2, \ldots K_T$, (which can be obtained from statistical data if available), the instability risk index RI_j in F_j defined by (20) can be further written as:

$$RI_j = \frac{\text{Unstable region in } F_j}{\text{Stable and Unstable regions in } F_j} = \frac{\sum_{i=1}^{K_U} \mu_i}{\sum_{i=1}^{K_T} \mu_i} \quad (21)$$

C. Impact of Charging Power on Stability Region of the DC Distribution System

It can be seen from Fig. 3 that the real parts of $\lambda_{\min k}$ and $\lambda_{\max k}$ determine the area of the stability region and the distance from the unstable region. The decrease in the real parts of $\lambda_{\min k}$ and$\lambda_{\max k}$ can increase the distance from the unstable region and thus, improve the stability of the DC distribution system.

From (14) and (A1) in Appendix A, the sum of the real parts of $\lambda_{\min k}$ and $\lambda_{\max k}$ is obtained as

$$SR_{\min k} = \sum_{i=1}^{6} \text{Re}[\lambda_{\min ik}] = \frac{P_{\min}}{C_{Lk} V_{Lk,0}^2} - \frac{\rho_k}{L_{fk}} - K_k$$
$$SR_{\max k} = \sum_{i=1}^{6} \text{Re}[\lambda_{\max ik}] = \frac{P_{\max}}{C_{Lk} V_{Lk,0}^2} - \frac{\rho_k}{L_{fk}} - K_k \quad (22)$$

where $K_k = (R_{Lk} + V_{fk,0} K_{Ipk} + R_{fk}) {L_{Lk}}^{-1}$.

It can be seen from (22) that if the charging power of all the EVCSs increases, $SR_{\min k}$ and $SR_{\max k}$ also increase, causing the stability region to move to the right side of the complex plane and increasing the instability risk of the DC distribution system. Conversely, if the charging power of all EVCSs decreases, the stability region moves to the left side of the complex plan, reducing the instability risk. Evidently, $SR_{\min k}$ and $SR_{\max k}$ in the charging state ($P_{Lk} > 0$) are considerably larger than in the discharging state ($P_{Lk} < 0$), which is why the EVCSs are at a greater risk of instability when they are operated in the charging state, rather than in the discharging state.

Increasing the $P_{\min}$ of the EVCSs causes the left boundary to move closer to the right, thereby narrowing the stability region. In the extreme case of all the EVCSs operating at the maximum charging power state, the left boundary is overlapped with the right boundary. In this case, all the oscillation modes are in the worst position of the stability region, indicating that the worst-case scenario of the DC distribution system is that all the EVCSs operate at the maximum charging state.

Similarly, decreasing the $P_{\max}$ of the EVCSs, causes the right boundary to move towards the left, and the stability region is far away from the unstable region, which increases the stability margin of the DC distribution system. Therefore, reducing peak charging power can improve the stability of the power system.

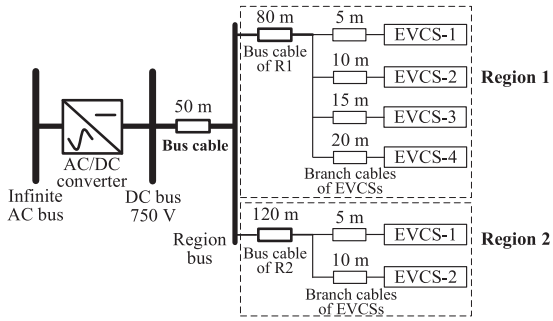

Fig. 4. Configuration of an example DC distribution system connected with 6 EVCSs.

D. Quick Evaluation of Instability Risk of the DC Distribution System

To estimate the instability risk of the DC distribution system, only the maximum and minimum charging power among the EVCSs are required. The highest dimension of matrices is reduced from 6*M* (Equation (6)) to 6 (Equation (14) and (19)). The method to detect the instability risk by using the proposed index of (20) can be summarized as follows.

1) Measure the minimum and maximum charging powers of the EVCSs, and establish a linearized model for them;
2) Establish the impedance matrix, **Z**, of the DC network and calculate the eigenvalues of **Z**;
3) Determine the left and right boundaries of the stability region and calculate RI_j in the frequency range F_j.
4) Set limitation of RI_j as $RI_{\lim}$, and sent warning messages to the administrators if $RI_j > RI_{\lim}$.

The proposed method is useful for engineers to quickly determine the stability region of a DC distribution system even if EVCSs operate in the stochastic state. Multiple complex scenarios are condensed into a simple scenario where only the minimum and the maximum charging states of the EVCSs should be detected, and thus significantly reduces the calculated load. The instability risk index, RI_j, is also meaningful in guiding the detection of the operation risk of the DC distribution system in real time.

The method proposed is much simpler than the traditional methods, such as the modal analysis and time-domain simulation [28]–[29]. It can be applied to the DC distribution system with any network topology. The proposed method is of great potential for the real-time detection of instability risk. Denote $T_{\lim}$ as the requirement of time to detect the instability risk in real time application. The method can be applied in real time in a large-scale DC distribution system as long as the time of calculating the index is less than $T_{\lim}$.

IV. Examples, Results and Discussions

Fig. 4 shows the configuration of a DC distribution system integrated with 6 EVCSs. The DC voltage at the DC bus is 750 V. The DC distribution system is connected to the AC power system via an AC/DC converter and is comprised of two charging regions. In each of the charging regions, there are 4 and 2 EVCSs

TABLE I
PARTIALLY CALCULATED RESULTS OF ρ_k, $\lambda_{\min 1k}$, $\lambda_{\max 1k}$, AND λ_{d1k}

k	ρ_k	$\lambda_{\min 1k}$	$\lambda_{\max 1k}$	λ_{d1k}
1	0.0046 + *j*0.0287	-6.1 + *j*1082	-1.6 + *j*1081	-1.62 + *j*1082
2	0.0052 + *j*0.0321	-6.9 + *j*1077	-2.17 + *j*1077	-2.2 + *j*1078
3	0.0058 + *j*0.0355	-7.4 + *j*1073	-2.7 + *j*1073	-2.72 + *j*1073
4	0.0067 + *j*0.0413	-8.4 + *j*1067	-3.6 + *j*1066	-8.1 + *j*1069
5	0.0194 + *j*0.1196	-20 + *j*977.0	-14 + *j*976.8	-17 + *j*991.7
6	0.0500 + *j*0.3089	-37 + *j*793.6	-31 + *j*793.4	-32 + *j*857.1

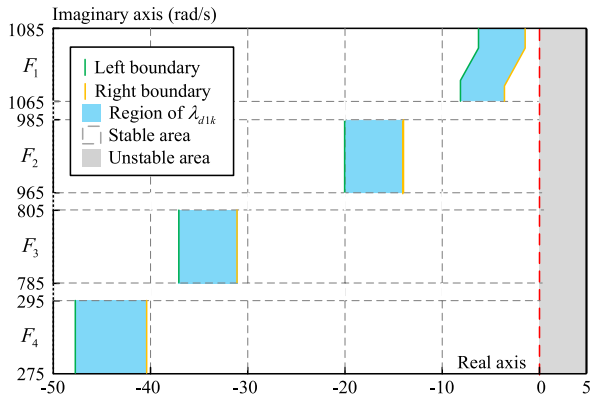

Fig. 5. Stability region of the DC distribution system.

respectively. Each region is connected to the DC bus through a bus cable, and each EVCS is connected to the region bus through the bus cable. Initially, the branch cable length of the first EVCS is 5 m, and the distance between two adjacent EVCSs is 5 m. Details of the cable lengths in the system are indicated in Fig. 4, and the other parameters are listed in Appendix C.

A. *Impact of the EVCSs' Charging Power*

In the tutorial case, the minimum ($P_{\min}$) and maximum ($P_{\max}$) charging powers of the EVCSs are 20 kw and 30 kw, respectively. Based on the parameters listed in Appendix C, the linearized models of the EVCSs are established separately with the minimum and maximum charging powers and the DC network. Table I lists the partially calculated results of ρ_k, $\lambda_{\min 1k}$, and $\lambda_{\max 1k}$. For verification, the realistic oscillation modes of the DC distribution system are provided in the last column of Table I.

Table I shows that $\lambda_{\min 1k}$ and $\lambda_{\max 1k}$ can be calculated by ρ_k instead of the complex transfer function of the DC network, which reduces the calculated load. Moreover, the realistic oscillation modes are located between $\lambda_{\min 1k}$ and $\lambda_{\max 1k}$, demonstrating that the stability region can cover all the locations of the realistic modes. Thus, all the oscillation modes can be calculated, forming the stability region of the DC distribution system, which is illustrated in Fig. 5.

It can be seen from Fig. 5 that the stability region is divided into multiple frequency ranges (F_1, F_2, F_3, and F_4), which are determined by the filter or control loops of the EVCSs. Because all the right boundaries of the region are on the left side of the

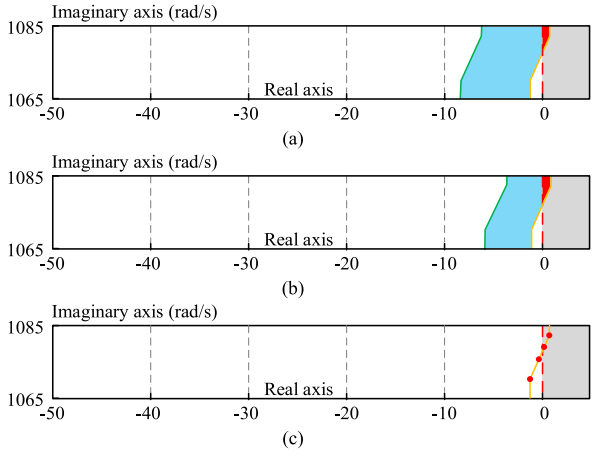

Fig. 6. Stability regions of the DC distribution system under the following conditions: (a) $P_{\max} = 35$ kW, (b) $P_{\min} = 25$ kW, (c) $P_{\min} = P_{\max} = 35$ kW.

unstable area, so that $RI_1 = RI_2 = RI_3 = RI_4 = 0$, there is no instability risk of the DC distribution system.

Moreover, increasing $P_{\max}$ from 30 to 35 kW, Fig. 6(a) shows that the stability region in the frequency range, F_1, of the DC distribution system moves towards the right side of the complex plane when compared to that in Fig. 5. In this case, a part of the region remains in the unstable area. This indicates that the DC distribution system faces the risk of the instability, and the instability risk index is calculated as $RI_1 = 3.6\%$. Furthermore, Fig. 6(b) demonstrates the stability region in the frequency range, F_1, upon increasing $P_{\min}$ from 20 to 25 kW. Here, the right boundary is rarely changed but the left boundary moves towards the right boundary, which narrows down the region and increases the instability risk to $RI_1 = 5.6\%$. Therefore, increasing the charging power of EVCSs creates a negative impact on the stability of the DC distribution system. The regions in other frequency ranges are not displayed as their instability risk is 0.

If $P_{\min}$ is increased such as that $P_{\min} = P_{\max} = 35$ kW, the oscillation modes of the DC distribution system are located on the right boundary of the stability region, as indicated by the red circles in Fig. 6(c). It can be seen from Fig. 6(c) that the two oscillation modes are located in the unstable area and thus, $RI_1 = 100\%$, indicating that the DC distribution system is unstable. The results confirm that the worst case scenario occurs when all of the EVCSs are operated at the maximum charging state. The sufficient condition for ensuring stability of the DC distribution system under the stochastic condition is holding the right boundary of the stability region in stable area. Therefore, the maximum charging power of each EVCS should not exceed 30 kW.

In order to demonstrate and evaluate the model proposed and analytical conclusions, simulation tests are conducted based on the SIMULINK software. Fig. 7 shows the results of the nonlinear simulations of two cases established using SIMULINK software based on the switch model. It can be seen that the DC distribution system is stable when the maximum charging power of the EVCSs is less than 30 kW (during the period

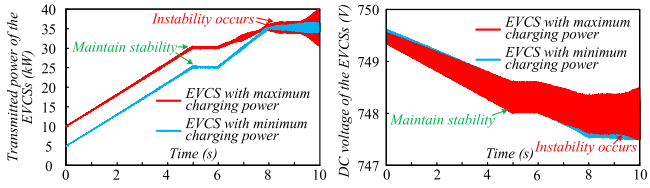

Fig. 7. Time-domain nonlinear simulation results (1).

TABLE II
LENGTHS OF BUS AND BRANCH CABLES OF R1

Bus cable length	Branch cable length of EVCSs	Total cable length
L_{bs} = 10 m	L_{e1} = 75 m	L_{t1} = 85 m
	L_{e2} = 80 m	L_{t2} = 90 m
	L_{e3} = 85 m	L_{t3} = 95 m
	L_{e4} = 90 m	L_{t4} = 100 m

1–6 s). However, with the increase in the transmitted power, the charging power of the EVCSs exceeds 30 kW, up to 35 kw, resulting in the instability of the DC distribution system. Therefore, the results confirm that the maximum charging power of the EVCSs should be limited to 30 kW and exceeding the limitation may lead to the instability of the DC distribution system.

B. Impact of the Connected Cable Length

As shown in Fig. 4, the distance between the EVCS and the DC bus is constant, so that the total length of the connecting cable between them is constant. Therefore, the bus cable length increases if the branch cable length decreases. Regarding the steady-state planning, the bus cable should be selected to be as long as possible to reduce the costs. However, the steady-state planning disregards the negative impact of the bus cable length on the stability of the DC distribution system. The importance of choosing the cable length is explained as follows.

The bus and branch cables of R1 are chosen as an example. The initial lengths of these cables are listed in Table II.

It can be seen from (21) that if the variation of the cable length makes ρ_k increase, the $SR_{\min k}$ and $SR_{\max k}$ decrease, causing the stability boundary to move to the left side of the complex plane and reducing the instability risk of the DC distribution system. Conversely, decreasing ρ_k increases the instability risk of the DC distribution system. Considering that the right boundary of the stability region is determined by the largest real parts of the oscillation modes, which correspond to the condition, $SR_{\max k} = P_{\max}(C_{Lk}V_{Lk,0}^2)^{-1} - \rho_{\min}{L_{fk}}^{-1} - K_k$, where $\rho_{\min}$ is the minimum value of ρ_k, we can evaluate the impact of cable length on the instability risk through $\rho_{\min}$. The smaller $\rho_{\min}$ is, the greater the probability that the right stability boundary is located in the unstable area, and the higher the instability risk.

By increasing the bus cable length of R1 from 10 to 70 m, the trajectory of $\rho_{\min}$ is calculated and illustrated, as indicated in Fig. 8 by the blue line. It can be seen that $\rho_{\min}$ decreases with an increase in the bus cable length of R1. Consequently, as indicated by the red line, the instability risk RI_1 increases,

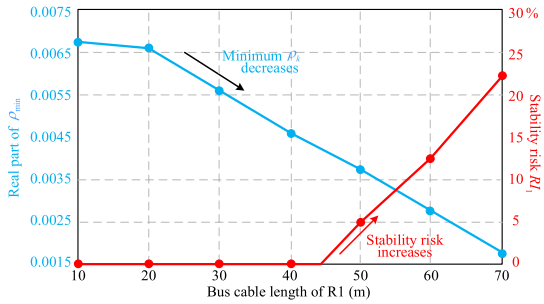

Fig. 8. Trajectories of $\rho_{\min}$ and RI_1 when bus cable length increases.

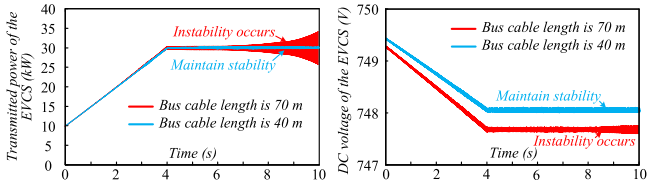

Fig. 9. Time-domain nonlinear simulation results (2).

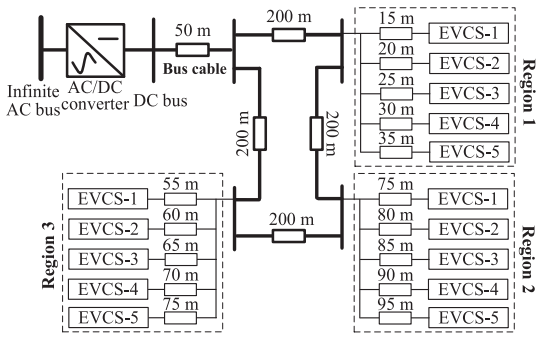

Fig. 10. Configuration of an example complex DC distribution system for EV charging.

thereby reducing the stability of the DC distribution system. The analysis results of Fig. 8 confirm that $\rho_{\min}$ can evaluate the impact of the DC network on the instability risk of the DC distribution system, and $\rho_{\min}$ should be increased to improve the stability of the DC distribution system. Therefore, increasing the bus cable length of R1 has an inverse impact on the dynamic characteristics and the steady state of the DC distribution system. Consequently, the cable length should be carefully designed considering its collective impact on the dynamic stability and the cost.

Fig. 9 shows the results of the non-linear simulations of two cases: case (1) and case (2), where the bus cable length of R1 is 70 m and 40 m, respectively. The charging power of the EVCSs in R1 increases from 0 to 30 kW during the period of 1–6 s. The results confirm that stability of the DC distribution system decreases when the bus cable length increases. Hence, to minimize the costs within the stability restrictions, the bus cable length should be chosen to be 40 m where the instability risk is 0.

C. A Complex DC Distribution System

Fig. 10 shows the configuration of an example complex DC distribution system integrated with 15 EVCSs in three areas.

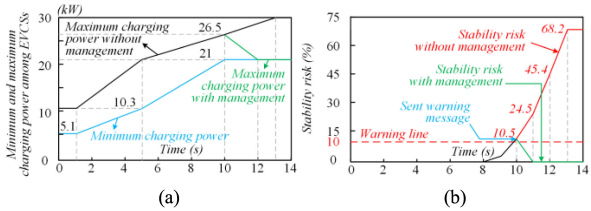

Fig. 11. Curves of the charging power (a) and the instability risk (b).

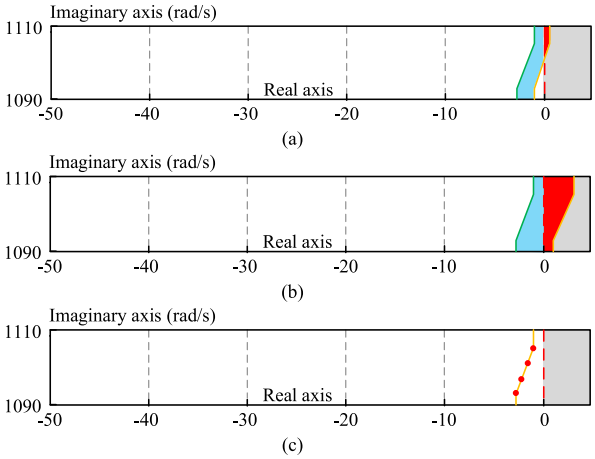

Fig. 12. Stability regions of the DC distribution system under the following conditions: (a) $P_{\max} = 26.5$ kW, $P_{\min} = 21$ kW, (b) $P_{\max} = 30$ kW, $P_{\min} = 21$ kW, (c) $P_{\max} = 21$ kW, $P_{\min} = 21$ kW.

There are 5 EVCSs in each area and the DC voltage at the DC bus is 750 V.

During the operation of 0–14 s, the charging power of all EVCSs is detected. The operating states of the EVCS with the minimum and maximum charging power are presented in Fig. 11(a). The charging power of the other EVCSs in the example DC distribution system is randomly variable.

At 10 s, $P_{\max}$ is increased to 26.5 kW and $P_{\min}$ remains at 21 kW, Fig. 12(a) shows the stability region in the frequency range, [1090, 1110] rad/s. It can be seen that part of the region remains in the unstable area. This indicates that the DC distribution system faces the instability risk. The instability risk index is calculated to be $RI_1 = 10.5\%$. Furthermore, Fig. 12(b) presents the stability region when $P_{\max}$ is increased to 30 kW at 13s. Here, the right boundary moves towards the right and the instability risk increases to $RI_1 = 68.2\%$. Therefore, increasing the charging power of EVCSs introduces a significant negative impact on the stability of the DC distribution system. To eliminate the instability risk, $P_{\max}$ can be limited. For example, by applying the limit that $P_{\min} = P_{\max} = 21$ kW, the oscillation modes of the DC distribution system are located on the left boundary of the region, as indicated by the red circles in Fig. 12(c). It can be seen from Fig. 12(c) that all oscillation modes are located in the stable region and thus, $RI_1 = 0\%$ such that the DC distribution system is stable.

Moreover, the instability risk in different frequency ranges is calculated. The highest instability risk at each operating point of the example DC distribution system is given in Fig. 11(b). Hence, a warning line can be set as $RI_{\lim} = 10\%$. If the instability risk exceeds $RI_{\lim}$, a warning message is issued to the operators to ensure that the monitoring and management of the entire DC distribution system can be enhanced. It is observed that during 0–8s, the DC distribution system is stable, and the instability risk is 0. The instability risk increases with the increase in the charging power. At 10s, the instability risk exceeds the warning line and thus, warning messages are sent out. Consequently, maximum charging power should be capped.

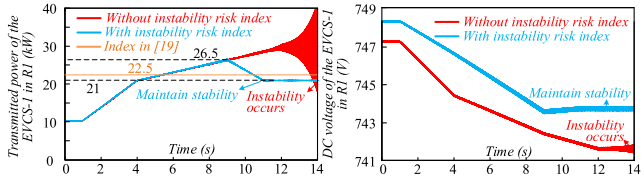

Fig. 13. Time-domain nonlinear simulation results (3).

Further discussions for comparison are as follows.

1) The modal analysis method based on the full-order model of a DC distribution system for the stability assessment is time-consuming and difficult to be applied for real-time detection of instability danger. For example, the maximum dimension of matrices involved in computation of the proposed index is 6th-order. Conversely, by applying the conventional method of modal analysis, the highest dimension of matrices involved in computation is increased with the increase in the scale of the DC distribution system.
2) The methods proposed in [10], [21] by assuming identical models of the EVCSs are restricted in application. For example, it can be seen from Fig. 11(a) that the operating states of the EVCSs are variable such that the instability risk is time-varying in real time. The situation can not be dealt with by the methods proposed in [10], [21].
3) A method that ignores the dynamics of the EVCSs and considers the EVCSs as constant power sources cannot detect the instability risk caused by the dynamics of the EVCSs. Nonlinear simulation results of a comparative study are presented in Fig. 13. It can be seen that the instability actually occurs if the index ignoring the entire dynamics of the EVCSs. Whilst, the instability risk is correctly detected by the proposed method in this study.
4) Compared with the instability risk index proposed in [20], the proposed index in the study is applicable for any topology of the DC network. Referring to [20], the charging power of the k^{th} EVCS should less than P_{Lim}, where $P_{Lim} = R_{fk}C_{fk}{V_{fk}}^2{L_{fk}}^{-1} = 22.5$ kW. However, it can be seen from Fig. 13 that the example DC distribution system remains being stable even if the charging power of the EVCSs increases to 26.5 kW. this demonstrates that the instability index proposed in [20] is applicable only for the network topology considered in [20].

V. Conclusion

The instability risk of a DC distribution system connected with EVCSs is evaluated in this study, by considering the stochastically varying operating state and the full dynamics of the EVCSs rather than assuming them to be identical and

modelled as constant power loads. A method to rapidly assess the instability risk is proposed, which involves the computation of reduced-order matrices. The proposed method is effective and applicable in a large-scale DC distribution system with a large number of EVCSs. The major conclusions and contributions of the study are summarized as follows.

1) The theoretical analysis demonstrates that a DC distribution system has higher possibility of instability if the EVCSs are in the charging state when compared to those in the discharging state. The instability risk of the DC distribution system increases with the increase in the charging power, and the system stability is the worst if all the EVCSs operate at the maximum charging state.
2) The bus cable length is a crucial factor affecting the stability of the DC distribution system. Thus, when the locations of the EVCSs are considered in the planning stage, the cable length should be carefully selected by considering the cost as well as the instability risk of the DC distribution system in operation.
3) This study proposes a method to quickly examine the instability risk of a DC distribution system, where the operating states of the EVCSs are stochastically varying. The proposed method requires only the information of the minimum and maximum charging powers among all the EVCSs, and the computation involves reduced-order matrices. The proposed method is demonstrated and evaluated based on two SIMULINK cases.

The correlation between the randomly varying states of the EVCSs may possibly be an important factor to affect the stability of a DC distribution system with the EVCSs. The paper calls upon to investigate the affecting factor, which certainly is the work that the authors shall explore carefully in near future.

APPENDIX A

Detail derivation results of (3):

$$\mathbf{\Delta X}_k = \left[\Delta V_{fk} \Delta i_{dck} \Delta V_{Lk}\ \Delta i_{Lk}\ \Delta x_{Vk}\ \Delta x_{Ik}\right]^T$$

$$\mathbf{A}_k = \begin{bmatrix} 0 & \frac{1}{C_{fk}} & \frac{i_{Lk,0}K_{Ipk}K_{Vpk}}{C_{fk}} \\ \frac{-1}{L_{fk}} & \frac{-R_{fk}}{L_{fk}} & 0 \\ 0 & 0 & \frac{P_{Lk}}{C_{Lk}V_{Lk,0}^2} \\ \frac{d_{Lk,0}}{L_{Lk}} & 0 & \frac{-(1+V_{fk,0}K_{Ipk}K_{Vpk})}{L_{Lk}} \\ 0 & 0 & -K_{Vik} \\ 0 & 0 & -K_{Iik}K_{Vpk} \end{bmatrix}$$

$$\begin{bmatrix} \frac{i_{Lk,0}K_{Ipk}-d_{Lk,0}}{C_{fk}} & \frac{-i_{Lk,0}K_{Ipk}}{C_{fk}} & \frac{-i_{Lk,0}}{C_{fk}} \\ 0 & 0 & 0 \\ \frac{1}{C_{Lk}} & 0 & 0 \\ \frac{-(R_{Lk}+V_{fk,0}K_{Ipk})}{L_{Lk}} & \frac{V_{fk,0}K_{Ipk}}{L_{Lk}} & \frac{V_{fk,0}}{L_{Lk}} \\ 0 & 0 & 0 \\ -K_{Iik} & K_{Iik} & 0 \end{bmatrix}$$

$$\mathbf{B}_k = \left[0\ 1/(L_{fk})\ 0\ 0\ 0\ 0\right]^T$$

$$\mathbf{C}_k = \left[0\ 1\ 0\ 0\ 0\ 0\right]^T$$

Fig. 14. Stability region of the DC distribution system in F_1.

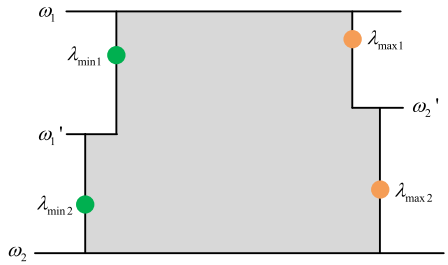

Fig. 15. Stability region of the DC distribution system in F_1 when two oscillation modes are considered.

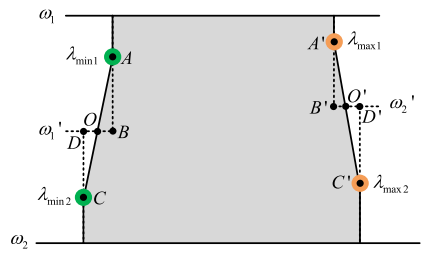

Fig. 16. Equivalent stability region of the DC distribution system in F_1.

APPENDIX B

Explanation of Fig. 3 is as follows.

Firstly, an oscillation mode in the frequency range $F_1 = [\omega_1, \omega_2]$ is considered. The oscillation mode at the minimum and maximum charging states is calculated to be $\lambda_{\min 1}$ and $\lambda_{\max 1}$, respectively. In this case, the stability region of the DC distribution system in F_1 is illustrated in Fig. 14.

Furthermore, two oscillation modes are considered in F_1. The oscillation modes at the minimum and maximum charging states are calculated to be $\lambda_{\min 1}$, $\lambda_{\min 2}$ and $\lambda_{\max 1}$, $\lambda_{\max 2}$, respectively. In this case, the stability region in F_1 is illustrated in Fig. 15.

In Fig. 15, $\omega_1' = \frac{\mathrm{Im}[\lambda_{\min 1}]+\mathrm{Im}[\lambda_{\min 2}]}{2}, \omega_2' = \frac{\mathrm{Im}[\lambda_{\max 1}]+\mathrm{Im}[\lambda_{\max 2}]}{2}$.

The stability region formed by directly connecting the oscillation modes is illustrated in Fig. 16. It is easy to see that the area of the stability region indicated in Fig. 15 equals to that in Fig. 16 because the area of ΔAOB and $\Delta AO'B'$equal to that of $\Delta COD$and $\Delta CO'D'$, respectively.

Generally, regarding the case of multiple oscillation modes in a selected frequency range, the boundary of the stability region can be formed by directly connecting neighboring oscillation modes. The area is as same as that of the stability region formed step by step. Hence, it is unnecessary to use curve fitting method for the discrete eigenvalue points.

APPENDIX C

TABLE III
PARAMETERS OF THE EVCSS IN THE DC DISTRIBUTION SYSTEM

Parameters of the EVCSs	Values (p.u.)
Capacitance of output filter of k^{th} DC/DC converter	$C_{fk} = 0.002F$
Inductance of output filter of k^{th} DC/DC converter	$L_{fk} = 0.0008H$
Resistance of output filter of the k^{th} DC/DC converter	$R_{fk} = 0.001\Omega$
Resistance of the line connecting the k^{th} DC/DC converter and battery	$R_{Lk} = 0.5\Omega$
Inductance of line connecting the k^{th} DC/DC converter and battery	$L_{Lk} = 0.01H$
Voltage-regulator capacitance of k^{th} battery	$C_{Lk} = 0.001F$
DC voltage across C_{Lk}	$V_{Lk} = 480V$
Transfer function of the outer voltage PI controller	$K_{Vpk} = 0.06, K_{Vik} = 300$
Transfer function of the inner current PI controller	$K_{Ipk} = 0.2, K_{Iik} = 1000$
Resistance and inductance of the transmission line per length	$0.0991\Omega / km, 0.5475mH / km$

REFERENCES

[1] B. Zhou, T. Littler, and L. Meegahapola, "Assessment of transient stability support for electric vehicle integration," in *Proc. IEEE Power Energy Soc. GE*, Boston, MA, USA, Nov. 2016, pp. 1–5.

[2] Q. Fu, W. Du, H. Wang, B. Ren, and X. Xiao, "Small-signal stability analysis of a VSC-MTDC system for investigating DC voltage oscillation," *IEEE Trans. Power Syst.*, vol. 36, no. 6, pp. 5081–5091, Nov. 2021, doi: 10.1109/TPWRS.2021.3072399.

[3] Q. Fu, W. Du, H. F. Wang, and B. Ren, "Analysis of small-signal power oscillations in MTDC power transmission system," *IEEE Trans. Power Syst.*, vol. 36, no. 4, pp. 3248–3259, Jul. 2021.

[4] W. Yao *et al.*, "A multi-objective collaborative planning strategy for integrated power distribution and electric vehicle charging systems," *IEEE Trans. Power Syst.,* vol. 29, no. 4, pp. 1811–1821, Jul. 2014.

[5] K. Qian, J. Gu, C. Zhou, Y. Yuan, X. Zhang, and H. Zhou, "Optimal planning of EV charging network based on fuzzy multi-objective optimisation," *CIRED - Open Access Proc. J.,* vol. 2017, no. 1, pp. 2462–2466, Oct. 2017.

[6] L. Yu, T. Jiang, and Y. Zou, "Distributed online energy management for data centers and electric vehicles in smart grid," *IEEE Internet Things J.*, vol. 3, no. 6, pp. 1373–1384, Dec. 2016.

[7] G. Wang *et al.*, "Robust planning of electric vehicle charging facilities with an advanced evaluation method," *IEEE Trans. Ind. Informat.*, vol. 14, no. 3, pp. 866–876, Mar. 2018.

[8] E. Veldman and R. A. Verzijlbergh, "Distribution grid impacts of smart electric vehicle charging from different perspectives," *IEEE Trans. Smart Grid*, vol. 6, no. 1, pp. 333–342, Jan. 2015.

[9] A. Y. S. Lam, Y. Leung, and X. Chu, "Electric vehicle charging station placement: Formulation, complexity, and solutions," *IEEE Trans. Smart Grid*, vol. 5, no. 6, pp. 2846–2856, Nov. 2014.

[10] W. Du, Q. Fu, and H. F. Wang, "Small-signal stability of a DC network planned for electric vehicle charging," *IEEE Trans. Smart Grid*, vol. 11, no. 5, pp. 3748–3762, Sep. 2020.

[11] M. Su, Z. Liu, Y. Sun, H. Han, and X. Hou, "Stability analysis and stabilization methods of DC microgrid with multiple parallel-connected DC–DC converters loaded by CPLs," *IEEE Trans. Smart Grid,* vol. 9, no. 1, pp. 132–142, Jan. 2018.

[12] M. Wu and D. D. Lu, "A novel stabilization method of LC input filter with constant power loads without load performance compromise in DC microgrids," *IEEE Trans. Ind. Electron.*, vol. 62, no. 7, pp. 4552–4562, Jul. 2015.

[13] A. Emadi, A. Khaligh, C. H. Rivetta, and G. A. Williamson, "Constant power loads and negative impedance instability in automotive systems: Definition, modeling, stability, and control of power electronic converters and motor drives," *IEEE Trans. Veh. Technol.*, vol. 55, no. 4, pp. 1112–1125, Jul. 2006.

[14] X. Lu, K. Sun, J. M. Guerrero, J. C. Vasquez, L. Huang, and J. Wang, "Stability enhancement based on virtual impedance for DC microgrids with constant power loads," *IEEE Trans. Smart Grid*, vol. 6, no. 6, pp. 2770–2783, Nov. 2015.

[15] L. Herrera, W. Zhang, and J. Wang, "Stability analysis and controller design of DC microgrids with constant power loads," *IEEE Trans. Smart Grid*, vol. 8, no. 2, pp. 881–888, Mar. 2017.

[16] J. Chen and J. Chen, "Stability analysis and parameters optimization of islanded microgrid with both ideal and dynamic constant power loads," *IEEE Trans. Ind. Electron.*, vol. 65, no. 4, pp. 3263–3274, Apr. 2018.

[17] W. Du, J. Zhang, Y. Zhang, and Z. Qian, "Stability criterion for cascaded system with constant power load," *IEEE Trans. Power Electron.*, vol. 28, no. 4, pp. 1843–1851, Apr. 2013.

[18] M. Tabari and A. Yazdani, "A mathematical model for a stability-enhanced DC distribution system for power system integration of plug-in electric vehicles," in *Proc. IEEE Power Energy Soc. Gen. Meeting*, Boston, MA, USA, Jul. 2016, pp. 1–5.

[19] J. L. Agorreta, M. Borrega, J. López, and L. Marroyo, "Modeling and control of N-paralleled grid-connected inverters with LCL filter coupled due to grid impedance in PV plants," *IEEE Trans. Power Electron.*, vol. 26, no. 3, pp. 770–785, Mar. 2011.

[20] M. Tabari and A. Yazdani, "A mathematical model for stability analysis of a DC distribution system for power system integration of plug-in electric vehicles," *IEEE Trans. Veh. Technol.*, vol. 64, no. 9, pp. 1729–1738, May 2015.

[21] Q. Fu, W. Du, and H. Wang, "Planning of the DC system considering restrictions on small signal stability of EV charging stations and comparison between series and parallel connections," *IEEE Trans. Veh. Technol.*, vol. 69, no. 10, pp. 10724–10735, Oct. 2020.

[22] MathWorks, "AC/DC three-level PWM converter," R2020b, Oct. 2020. [Online]. Available: https://www.mathworks.com/help/physmod/sps/ug/ac-dc-three-level-pwm-converter.html?s_tid=srchtitle

[23] MathWorks, "Bidirectional DC-DC converter," R2020b, Oct. 2020. [Online]. Available: https://www.mathworks.com/help/physmod/sps/ref/bidirectionaldcdcconverter.html?searchHighlight=DC%2FDC&s_tid=srchtitle

[24] P. Liutanakul, A. Awan, S. Pierfederici, B. Nahid-Mobarakeh, and F. Meibody-Tabar, "Linear stabilization of a DC bus supplying a constant power load: A general design approach," *IEEE Trans. Power Electron.*, vol. 25, no. 2, pp. 475–488, Feb. 2010.

[25] T. F. Wu, C. H. Chang, L. C. Lin, G. R. Yu, and Y. R. Chang, "DC-bus voltage control with a three-phase bidirectional inverter for DC distribution systems," *IEEE Trans. Power Electron.*, vol. 28, no. 4, pp. 1890–1899, Apr. 2013.

[26] W. Du, W. K. Dong, and H. F. Wang, "Small-signal stability limit of a grid-connected PMSG wind farm dominated by the dynamics of PLLs," *IEEE Trans. Power Syst.*, vol. 35, no. 3, pp. 2093–2107, May 2020.

[27] C. D. Meyer, *Matrix Analysis and Applied Linear Algebra*. Philadelphia, PA, USA: SIAM, 2000.

[28] W. Du, Y. Wang, Y. Wang, H. F. Wang, and X. Xiao, "Analytical examination of oscillatory stability of a grid-connected PMSG wind farm based on the block diagram model," *IEEE Trans. Power Syst.*, early access, 2021.

[29] W. Du, Y. Wang, H. F. Wang, X. Xiao, X. Wang, and X. Xie, "Analytical examination on the amplifying effect of weak grid connection for the DFIGs to induce torsional sub-synchronous oscillations," *IEEE Trans. Power Del.*, vol. 35, no. 4, pp. 1928–1938, Jul. 2020.